Structure and Thermodynamics of Grafted Three-Arm Branched Polymer Layers

M. A. Carignano* and I. Szleifer*

Department of Chemistry, Purdue University, West Lafayette, Indiana 47907

Received July 13, 1993; Revised Manuscript Received November 8, 1993⊛

ABSTRACT: The conformational and thermodynamic behavior of grafted polymer layers composed of linear and three-arm branched chains, with one branch grafted to the surface and two free branches of equal length, in the good solvent regime are investigated. The molecular organization of the layers composed of branched chains with a long branch grafted to the surface and two short free branches is very similar to that of linear chains. However, as the branch grafted to the surface becomes shorter, for the same total number of segments per chain, the conformational behavior of the chains changes markedly, in particular for high surface coverages. The density of the free end segments for chains with a short grafted branch shows two maxima, one near the solvent side of the brush and the other near the grafting wall. It is found that at high surface coverages the chains organize such that the short grafted branch is very highly stretched, one of the free branches is predominantly stretched toward the solvent while the other free branch folds toward the grafting wall. The force between two parallel grafted layers is calculated as a function of the distance between the grafted walls. The interactions between grafted surfaces with branched chains are more steeply repulsive than those for linear chains. Moreover, the interdigitation and the changes in molecular organization as the layers approach each other are studied for the different chain architectures.

1. Introduction

Grafted polymeric layers, usually called polymer brushes, are currently used as surface modifiers and have been the subject of intensive investigations during the last decade. A variety of technological problems such as colloidal stability, adhesion, etc., are strongly related to the properties of the polymer layer, and consequently, to the conformations of the constituent chains.

Experimental approaches to the study of polymer brushes have included the measurement of the polymer concentration profile by evanescent wave techniques,[1] neutron reflectivity[2,3] and neutron scattering,[4,5] as well as the direct measurement of the force as a function of the distance between two coated surfaces.[6,7] More recently, measurements of surface pressure isotherm have been reported.[8] Polymer brushes composed of linear chains grafted on planar surfaces and immersed in a good solvent are today a problem well understood. Scaling approaches,[9-11] self-consistent field (SCF) theories,[12-23] and computer simulations[24-28] have been developed to predict the properties of the polymeric layer. The predictions from these theories have shown good agreement with the experimental observations of the density profile as well as force profiles. However, they do not seem to properly describe the recently measured pressure isotherms.[8] For an overview we direct the reader to three recents reviews[21,29,30] where most of the theoretical and experimental work is summarized.

Grafted layers composed of star polymers may have interesting and useful properties from a practical point of view. The presence of more than one end per chain could be a way to improve the practical applications that depend on end functionalized groups, e.g. chemical reactivity.[31,32] For example, as will become clear later, for certain chain architectures the distribution of end segments throughout the layer shows important qualitative differences with that of the linear chain. Also, the interactions between grafted surfaces turn out to be strongly dependent on the type of grafted branched chain. This may have important consequences in the use of different chain architectures for colloidal stabilization.[33] Furthermore, the understanding of the conformational properties of branched polymers in the inhomogeneous environment created by the surface is a challenging theoretical problem.

In a recent paper we have presented a theoretical approach to study the conformational and thermodynamic properties of grafted polymeric layers.[34] The theory is a "single-chain" mean-field approximation in which one looks at a central chain in the mean field of the interactions with the other molecules of the environment, namely the solvent and other chains. The central quantity of the theory is the probability distribution function (pdf) of chain conformations. With the help of the pdf one can calculate any average conformational or thermodynamic property. The pdf turns out to be determined by the osmotic pressures due to the requirement to keep constant the chemical potential of the solvent throughout the layer. The osmotic pressures, and thus the pdf and the polymer and solvent density profiles, are determined by the constraint imposed by the assumption that the layer is incompressible. In order to obtain the pdf the theory requires the set of configurations of a single grafted chain. Then, the same set of single-chain conformations can be used to solve for all grafting densities and qualities of solvent. In this approach, the introduction of the chain's architecture, whether linear, branched, or any other desired type, is straightforward through the set of single-chain configurations. The low computational cost needed to solve the problem once the chains are generated, allows us to do systematic studies as the one described in this work.

In the first application of the theory[34] to grafted polymer layers we have studied the behavior of linear chains in good solvent for a variety of chain lengths and models. For linear chains, our approach shows excellent quantitative agreement with the molecular dynamics simulations of Murat and Grest for all grafting densities.[25] Moreover, they also show agreement in the scaling behavior of the density profile and film thickness with the analytical SCF theories.[19,22] However, this agreement was shown not to hold for the polymers free energy.[34]

⊛ Abstract published in *Advance ACS Abstracts*, December 15, 1993.

0024-9297/94/2227-0702$04.50/0 © 1994 American Chemical Society

We have also reported[34] preliminary results for branched molecules modeled in a cubic lattice and of relatively short length. The conclusions from that work were that the behavior of grafted short branched chains does not show any qualitative difference with linear chains. However, as will become clear this is not the general case and it is the result of the short molecules studied there.

In this paper we investigate the structural and thermodynamics properties of polymer brushes composed of three-arm branched chains in good solvent conditions. One of the three arms has the end grafted to a planar surface, and the other two branches are free. We present a systematic study of an off-lattice chain model of total length $n = 50$, for a variety of chain architectures. For all chain architectures the structural and thermodynamic properties were calculated for a variety of grafting densities covering the whole spectrum of possibilities from very low to very high surface coverages. Our findings show that the molecular organization of the films, as well as their thermodynamic behavior, is strongly dependent on the chain architecture.

The paper is organized as follows. In section 2 the theory is derived in an alternative way to that presented in ref 34. The details of the chain model used in the application of the theory are also described. Section 3 presents the results obtained from the theory for a variety of chain architectures and surface coverages. Finally, section 4 summarizes our findings and main conclusions for possible experimental measurements to check the validity of our calculations.

2. Theoretical Background

The derivation of the theory shown in this section is based upon the minimization of the Helmholtz free energy of the system subject to the packing constraints imposed by the assumption of incompressibility. This derivation differs from the one presented in ref 34. In that paper we obtained the pdf of chain conformations and the density profiles through an expansion of the canonical partition function of the system. Even though the derivation presented here is simpler, it provides exactly the same results. However, the longer derivation of ref 34 allows one to visualize better the approximations done in the derivation of the theory. The reader is referred to that paper for more details.

We consider a system of N_p polymer molecules grafted by one end to an impenetrable, purely repulsive, surface of total area $a(0)$. The polymer layer is embedded in a solvent composed of N_s molecules. We model the polymer molecule as a chain composed of n connected segments each of volume v_0, and we consider that the volume of the solvent molecule is also v_0. The coordinate system is defined with the z axis normal to the surface so that the chains are in the positive z side, Figure 1. The symmetry of the problem implies that the system is uniform at each plane orthogonal to the z axis, so that the positive z direction is only relevant for the inhomogeneous arrangement of polymer and solvent densities. The basic assumption of the theory is that the polymer–solvent layer is incompressible, so that the total fluid density is constant. We concentrate our analysis on how the polymer chains and the solvent molecules share the volume available to them at each layer of thickness dz at position z. The layer's incompressibility imposes a constraint on the polymer and solvent volume fractions at each concentric layer parallel to the interface. This volume filling constraint is mathematically expressed as

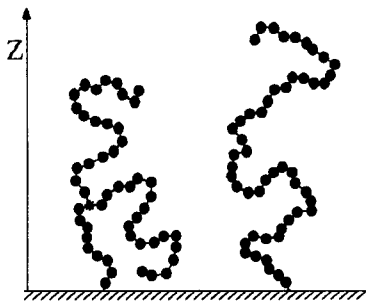

Figure 1. Schematic drawing of branched (right) and linear (left) chains grafted to a solid surface, both with 50 segments. The branched molecule is called B10; i.e. the grafted branch has 10 segments and the two (symmetric) free branches have 20 segments each. The star in the B10 chain marks the branching segment. The coordinate system used throughout the paper is also displayed.

$$\langle \phi_p(z) \rangle + \langle \phi_s(z) \rangle = 1 \qquad z \geq 0 \tag{1}$$

where $\langle\ \rangle$ denote ensemble average, the first term is the average polymer volume fraction, and the second term is the average volume fraction of the solvent, both at layer z. It should be recognized that eq 1 accounts, in an average way, for the repulsive interactions (excluded volume) between different volume units.

The polymer volume fraction at layer z is related to the average number of polymer segments per chain $\langle n(z) \rangle dz$ at the same layer by

$$\langle \phi_p(z) \rangle = \sigma \langle n(z) \rangle v_0 \tag{2}$$

where $\sigma = N_p/a(0)$ is the number of grafted polymer molecules per unit area (polymer surface coverage). The average number of segments of polymer in layer z can be written as

$$\langle n(z) \rangle\ dz = \sum_{\{\alpha\}} P(\alpha) n_\alpha(z)\ dz \tag{3}$$

where $P(\alpha)$ is the pdf of chain conformations, $n_\alpha(z)dz$ is the number of segments that the chain in conformation α has at layer z, and $\{\alpha\}$ means that the sum runs over all the possible conformations of a single chain. It should be stressed that the pdf is a function of the surface coverage σ. It is also convenient to introduce the number density of solvent molecules, $\rho_s(z)$, which is related to the solvent volume fraction by

$$\langle \phi_s(z) \rangle = \rho_s(z) v_0 \tag{4}$$

Let us consider the good solvent regime. The generalization of the equations presented here for other qualities of solvent is straightforward, as shown in refs 34 and 35. In the good solvent regime we can assume that the only relevant interactions in the system are the short range repulsions that we model as excluded volume interactions. These are taken into account through the volume filling constraints, eq 1. Now we are interested in the Helmholtz free energy per unit area, A/a, of the system. We can write this free energy in the form

$$A/a = \sigma A_p + \int \rho_s(z) A_s(z)\ dz \tag{5}$$

where A_p is the Helmholtz free energy per polymer molecule and $A_s(z)$ is the Helmholtz free energy per solvent molecule at layer z. The free energies include an entropic and an energetic term. However, in the good solvent limit the system becomes athermal and therefore there are only entropic contributions to A. Explicitly, the free energy

density can be written as

$$\beta\frac{A}{a} = \sigma\sum_{\{\alpha\}}P(\alpha)\ln P(\alpha) + \int_0^\infty dz\ \rho_s(z)[\ln(\rho_s(z)v_0) - C] \quad (6)$$

where $\beta = 1/kT$, with k the Boltzmann constant and T the absolute temperature. The first term comes from the configurational entropy of the chains, expressed in terms of the pdf of chain conformations, the second one is the mixing (translational) entropy of the solvent, and C is an arbitrary constant. Note that the last term in eq 6 is equal to the constant C multiplied by the total number of solvent molecules per unit area, i.e., CN_s/a. This is an additive constant to the free energy that has no thermodynamic implication. The entropic contribution arising from the chain molecules does not have a translational component due to the fact that we consider the polymers to be grafted to the surface. Note that if we were interested in mobile chains we could include the translational contribution in a mean-field approximation, i.e. proportional to $\ln \sigma$; however, this term will have no influence either in the pdf of chain conformations or in the solvent density profile.[35]

The "best" $P(\alpha)$ and $\rho_s(z)$ are those that minimize the Helmholtz free energy, eq 6, subject to the constraints, eq 1. These can be simply obtained by introducing the Lagrange multipliers $\beta\pi(z)$, which give for the pdf of chain conformations

$$P(\alpha) = \frac{1}{q}\exp[-\int_0^\infty dz\ \beta\pi(z)v_0n_\alpha(z)] \quad (7)$$

where q is the normalization constant that ensures $\sum_{\{\alpha\}}P(\alpha) = 1$. For the solvent density we get

$$\rho_s(z)v_0 = \exp[-\beta\pi(z)v_0 + C] \quad (8)$$

The volume filling constraints, eq 1, with the expressions for $P(\alpha)$ and $\rho_s(z)$ are sufficient to determine all the properties of the system. In order to interpret the significance of the Lagrange multipliers $\pi(z)$ we note that they have the units of pressure. Moreover, eq 8 suggests that these are osmotic pressures provided that the constant C is the chemical potential of the solvent throughout the layer, μ_s. This, indeed, is the result derived from the partition function as detailed in ref 34. It should be stressed that the chemical potential of the solvent should be constant at all z layers in order to have thermodynamic equilibrium. Thus, $\pi(z)$ are the osmotic pressures that arise in order to keep μ_s constant in the regions where the solvent is "mixed" with the polymer molecules.

The only unknowns in the problem to solve the constraint equations with the pdf and the solvent density profile that minimize the free energy are the osmotic pressures, $\pi(z)$. The equations to be solved are obtained by grouping eq 1 with eqs 2, 3, 7, and 8,

$$\sigma\sum_{\{\alpha\}}\frac{1}{q}e^{[-\int_0^\infty dz'\beta\pi(z')v_0n_\alpha(z')]}n_\alpha(z)v_0 + e^{-\beta\pi(z)v_0+\beta\mu_s} = 1 \qquad z \geq 0 \quad (9)$$

where σ and μ_s are the parameters that define the thermodynamic state of the system. Namely, for a given chain architecture one needs to know the complete set (or a representative sample) of the single chain configurations and then solve for any desired value of σ. As shown in the Appendix the value of the solvent chemical potential is irrelevant to the determination of the density profiles and the pdf.

From the expressions for $P(\alpha)$ and $\rho_s(z)$ we can express the Helmholtz free energy per unit area A/a, in terms of the osmotic pressures

$$\beta\frac{A}{a} = -\sigma[\ln q + \int_0^\infty \beta\pi(z)v_0\langle n(z)\rangle\ dz] - \int_0^\infty \beta\pi(z)v_0\rho_s(z)\ dz \quad (10)$$

where the first term comes from the chains free energy and the second is the solvent contribution. Replacing the solvent density in terms of the polymer volume fraction by means of the constraint equations, eq 1, one obtains

$$\beta\frac{A}{a} = -\sigma\ln q - \int_0^\infty \beta\pi(z)\ dz \quad (11)$$

where the normalization of the pdf is explicitly given by

$$q = \sum_{\{\alpha\}}\exp[-\int_0^\infty dz\ \beta\pi(z)v_0n_\alpha(z)] \quad (12)$$

2.1. Chain Model. As discussed following eq 9 we need to generate all the possible (or an appropriate sample) single-chain conformations for a given polymer architecture. We use the rotational isomeric state (RIS) chain model,[36] where each bond can have three possible states: trans, gauche+, and gauche− with angles $\varphi = 0$, 120, and −120°, respectively, and with the angle between bonds $\theta = 68°$. Linear molecules and four differents types of three-branched chains are considered, all of them of total length $n = 50$ segments, with bond length l. The branched chains are called B10, B20, B30, and B40, where the number indicates the position of the branched segment from the grafting point. For example, the chain B10 consists of a grafted branch of 10 segments and two tails of 20 segments each connected to segment 10 (see Figure 1). The segments are counted from the one grafted to the surface. In the branched chains once the grafted arm is generated then from the branching segment the two free arms are grown, each one in a different orientation with respect to the other. Thus, the branching bond has two configurations, i.e. t/g+, t/g−, or g+/g−, one for each of the first bonds of the two free arms. Then the rest of the two arms are generated in the usual way. All the linear and branched chains are fully flexible. Namely, we assume that there is no energetic difference between the different states of each bond. It should be kept in mind that a segment of our model chains represents a few units of real polymer molecules.[37] Moreover, the effects of flexible vs semi-flexible chains was already studied for linear chains in ref 34.

In order to solve eq 9 we discretize the space in layers of finite thickness δ so that we can count the number of segments per layer for each accepted conformation. Therefore, we have converted the integral equations into a set of nonlinear coupled equations

$$\frac{\sigma}{\delta}\sum_{\{\alpha\}}\frac{1}{q}e^{-\sum_{i=0}^{M}\pi_in_\alpha(i)}n_\alpha(j) + e^{\mu_s-\pi_j} = 1 \qquad 1 \leq j \leq M \quad (13)$$

where M is the total number of layers taken so that the fully extended chain cannot reach the last layer M. π is measured in kT/v_0 units, $n_\alpha(i)$ is in v_0 units, σ is in $1/l^2$ units, and μ_s is in kT units. Equation 13 is solved by standard numerical methods. We have obtained identical results by varying the thickness of the layer δ from $1.0l$ to $2.0l$.[34] We have chosen $\delta = 1.86l$ for practical reasons. For the chemical potential of the solvent we have assumed $\mu_s = 0$, as in a pure mean field solvent that completely fills the available volume; see the Appendix for further discussion of this point.

The summation in eq 13 runs over all the possible conformations of the chain. It is impossible to generate

them for chains of length $n = 50$, but we can solve the constraint equations and obtain a good solution by taking a representative sample of the complete set of conformations. We have used a simple sampling method with which we generate 2.85×10^6 accepted conformations. Each conformation is characterized by a randomly chosen bond sequence, trans, gauche+, and gauche−, and a random overall orientation with respect to the surface. The branching bond has two random configurations, as explained above. The accepted conformations have all their segments in $z > 0$ and they are all self-avoiding; i.e., no two nonbonded segments can be at a distance shorter than the bond length, l. For each accepted conformation we calculate the set of numbers $\{n_\alpha(i)\}$ necessary to solve eq 13, and all the desired conformational properties as presented in section 3. Once the osmotic pressures are determined, the average properties of the chains are calculated using the pdf, $P(\alpha)$, as given in eq 7. For example the average number of polymer segments in layer 1 is obtained by

$$\langle n(1) \rangle = \sum_{\{\alpha\}} P(\alpha) n_\alpha(1) \qquad (14)$$

3. Results

We have studied the behavior of the five chain architectures for a variety of grafting densities. In this section we show the most important results concerning the differences and similarities between the different polymer chains. All the results are in the good solvent regime.

Figure 2 shows the density profile for the systems composed of branched B10, B20, B30, and B40 and of linear chains, for three different grafting densities, σ = 0.03, 0.10, and 0.15 corresponding to low, intermediate, and high surface coverages, respectively. The density profile of the B40 branched system in practically identical to that of the linear chains for all the grafting densities. This similarity is in line with our earlier results on shorter chains with short free branches.[34] The other chain architectures, B30, B20, and B10, show a marked difference in the density profiles as compared to the linear one. The differences become more pronounced as the surface coverage increases. In general the B30, B20, and B10 systems have a shorter profile with a higher value of the density at the plateaulike region. This reflects the more compact structure of the starlike molecules than the linear ones and also the fact that the branched chains have a maximal extension (perpendicular to the grafting surface) that is given by $25 + i/2$, where i is the number of segments of the grafted branch. Note that for a given surface coverage the area under the density profile is equal for all chain architectures.

A well-known result for linear chains[20,25] is that there is a qualitative change in the shape of the density profile from a parabolic-like shape at intermediate σ to one close to a step function when the surface coverage increases to very high values. This qualitative change in the profile also appears in the branched systems. However, the crossover seems to occur at a lower value of σ than in the linear chains system, again reflecting that the branched chains are "bulkier" than the linear ones. Furthermore, the branched systems show a nonmonotonic variation of the profile, even after the initial increase of density very near the grafting wall. The B10 brush has a maximum at $z/l \sim 8$ for $\sigma = 0.10$ and $\sigma = 0.15$, and B20 has an analogous maximum at $z/l \sim 14$ for $\sigma = 0.15$. The reason for these maxima is the presence of the branching point, that is very localized at these grafting densities at the positions where the maximum occurs.

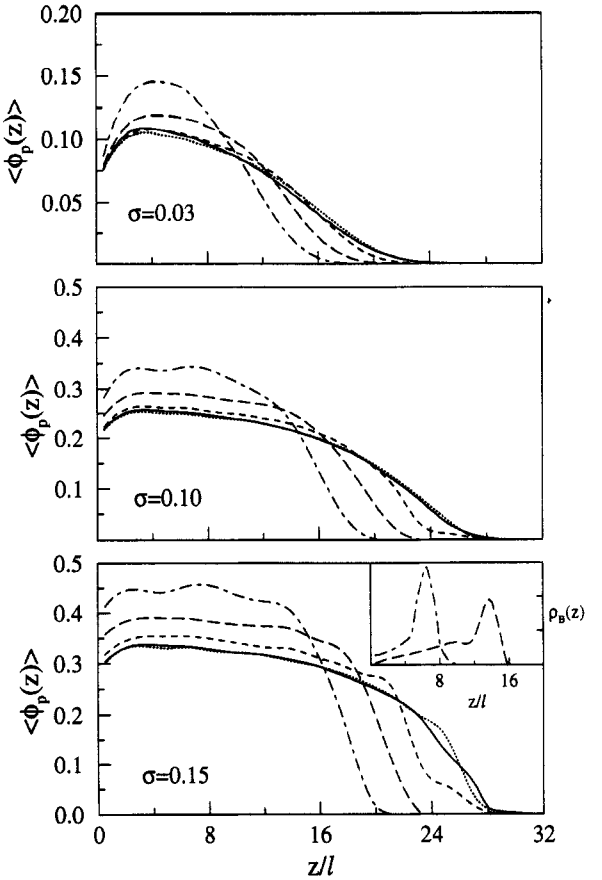

Figure 2. Polymer volume fraction as a function of the distance from the grafting wall for five different chain architectures: linear chains (full lines); B40 (dotted lines); B30 (short dashed lines); B20 (long dashed lines); B10 (dotted-dashed lines). The three graphs correspond to the different grafting densities, σ, marked on the lower left corner. Note the different scale for $\sigma = 0.03$. The inset in the lower plot shows the distribution of the branching segment for B10 chains (dotted-dashed line) and B20 chains (long dashed line) as a function of the distance from the grafting wall. Note that the distributions are narrow and the locations of their maximum are at the same distance from the walls, z/l, as the bump in the corresponding density profiles.

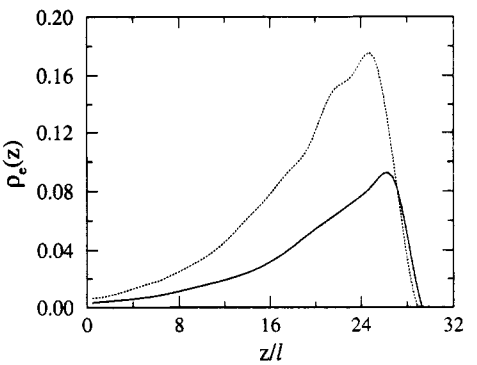

Figure 3. Density of free ends as a function of the distance from the grafting wall for linear (full line) and B40 (dotted line) chains, both for $\sigma = 0.15$. Note that the integral under the B40 profile is twice that of the linear chain due to the fact that the branched chains have two free ends per chain.

As mentioned above the behavior of the B40 chains is very similar to that of the linear ones for almost all their conformational properties. However, the B40 chains have two free ends and therefore the question that arises whether the end distribution of these branched chains is similar to that of the linear ones. Figure 3 shows the density of the free ends of the chains as a function of the distance from the grafting wall for $\sigma = 0.15$. Note that the integral of the curve for B40 is equal to 2 whereas the

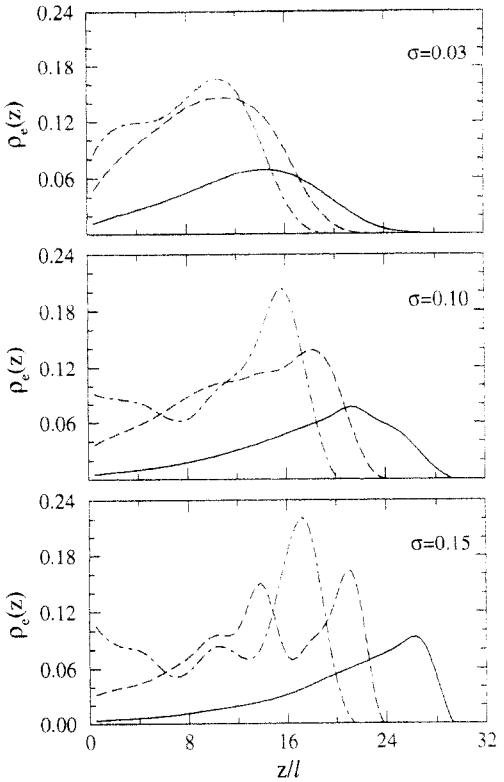

Figure 4. Density of free ends as a function of the distance from the interface for linear, B20, and B10 chains (lines are as in Figure 2) for the same three surface coverages as shown in Figure 2.

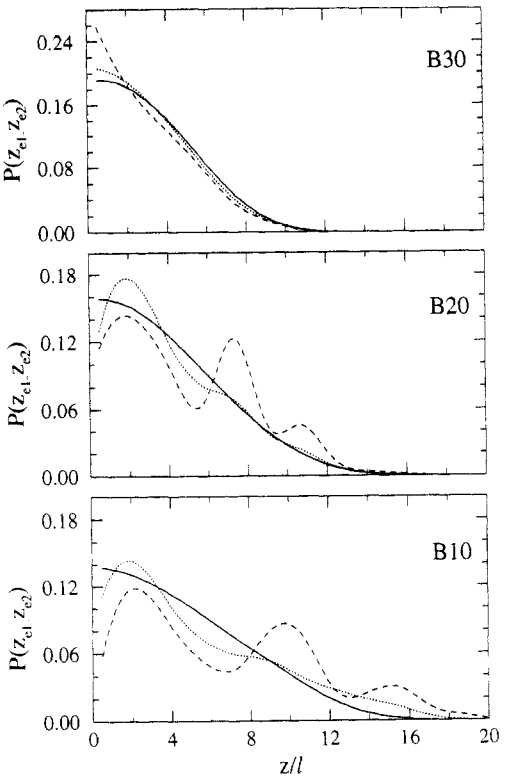

Figure 5. Probability distribution of the normal component (with respect to the grafting wall) of the separation between the two free ends for B30, B20, and B10 chains, for three different surface coverages: σ = 0.03 (full lines); σ = 0.10 (dotted lines); σ = 0.15 (dashed lines). Note the different scale of the probability axis for the B30 chains.

integral for the linear chain is 1. The shape of the profiles for the two chains architectures is very similar. This is true for all the surface coverages that we have studied. However, the B40 chain has double the number of end groups and therefore it may prove to be useful for applications in which functionalized free ends are desired.

The density of end groups for the shorter branched chains shows important qualitative differences with that of the linear chains. This is shown in Figure 4 for three different grafting densities. The qualitative behavior of the end group density is now a function of chain architecture and grafting density. For low surface coverages the linear and B20 chains show similar shapes of the profile, the only difference between them has to do with the shorter dimension of the B20 chain. The B10 chain, however, shows a different shape in which the probability of finding a free end is largely increased close to the grafting surface. As the surface coverage is increased the linear chains have the maximum of the distribution shifted far from the grafting wall due to the stretching of the chains. This result was already explained by several groups using SCF approaches[20,38] and computer simulations.[25,27] The density of ends for the B10 and B20 chains does not follow exactly the same behavior. For both branched chains there is an increase of the density of ends far from the grafting surface. However, there is also the appearance of an additional (or two additional for the highest surface coverage) maximum in the distribution. In order to understand the different qualitative behavior of the branched chains as manifested in the density of free ends, it is useful to look at additional conformational information.

The question that arises, due to the nonmonotonic behavior of the distributions, is how the two free ends in the branched chains are distributed. To this end, we show in Figure 5 the probability distribution for the normal component of the distance between the two free ends of the chains, $P(z_{e1} - z_{e2})$, for the branched B10, B20, and B30 molecules for the same surface coverages as in Figure 4. The B30 chain, which is the one with relatively short free branches, shows that the probability of finding the two ends at a given distance normal to the surface decreases monotonically with the separation, and also it has its maximum at zero separation. These results imply that most of the chains have the two free branches symmetric to each other for all surface densities. This is confirmed by looking at the same distribution for the other segments of the free branches, not shown here. This is clearly understood from the fact that the two branches are not long enough to be able to have the ability to have the two ends at very large distances. The picture changes qualitatively for the two other branched chains with longer free branches. In both cases the shape of the distribution function develops from a monotonically decreasing function, at low surface coverages, to one with a marked maximum at a finite (non-zero) separation with another peak starting to appear for intermediate grafting densities. Finally, the high surface coverage distributions show three marked maxima. The differences between the B20 and B10 chains are only quantitative and show just that the peaks are broader and shifted toward larger separations for the B10 chains because the two free branches are longer. Looking in detail at the location of the three maxima in B20 and B10, they correspond to the separations between the different maxima in the densities of end groups, as shown in Figure 4. These results suggest that for the chain molecules with long free branches the probability of the conformations having one end toward the grafting wall while the other free end is stretched toward the solvent becomes very large. This is further confirmed by looking at the distribution of free ends of one of the branches when the other branch has its end within a distance $1.5l$ from the grafting wall. This distribution (not shown here) shows that most of the probability of the second free end has a very sharp maximum very near the pure solvent,

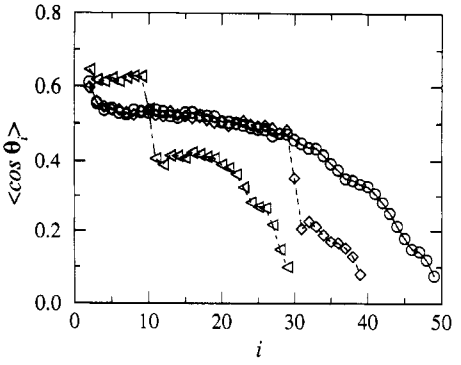

Figure 6. Average orientation of the bond as a function of the segment number i for linear (circles), B30 (diamonds), and B10 (triangles) chains, all for $\sigma = 0.10$. The orientation is measured by $\langle \cos \theta_i \rangle$ where θ_i is the angle between the line connecting segments $i + 1$ and $i - 1$ and the normal to the grafting wall. Note that for the branched chains the number of segments shown is less than the total chain length. This is so because the two free branches have the same average orientation. Therefore, for the B10 (B30) chains the profile from $i = 31$ (41) to $i = 50$ is identical to that from $i = 11$ (31) to $i = 30$ (40).

namely at $z/l \simeq 21$ and 17 for the B20 and B10 chains, respectively, for $\sigma = 0.15$.

The next question that arises is how do the B20 and B10 chains organize at high surface coverages so that the two free branches have a high probability to go in "opposite" directions. In order to understand that it is useful to look at the orientation of the segments with respect to the interface. These can be quantitative measured by $\langle \cos \theta_i \rangle$, where θ_i is the angle between the line connecting segments $i + 1$ and $i - 1$ and the normal to the interface. We take this particular angle to avoid the odd–even effect that is obtained in the RIS chains.[36] Then, $\langle \cos \theta_i \rangle = 1$ means that the segment i is perpendicular to the surface for all the conformations whereas $\langle \cos \theta_i \rangle = 0$ implies a completely random orientation of the segment. Figure 6 shows the orientation of the segments as a function of the segment number for the linear, B30, and B10 systems at $\sigma = 0.10$. The orientation of the linear chains decreases monotonically with the segment number. The last few segments are the most randomly oriented, but they do not reach the zero value of $\langle \cos \theta_i \rangle$ because they still feel the stretching of the chain. This behavior of the linear chains in good solvents was already described by several groups.[25,27] The branched chains orientation suffers a jump down just in the branching segment. The orientation of the segments in the free branches is similar to the equivalent last segments of the linear chain. The "discontinuity" in the orientation profiles reflects the spreading experienced by the two free branches due to the presence of the knot where the local density of segments is very high, as shown in the density profiles (Figure 2). Namely, in order to accommodate the two free branches the segments must be much less aligned due to strong repulsions than they would be otherwise. The systems B40 (not shown in the figure) and B30 follow the curve of the linear chains for all segments of the grafted branch. The orientation is more pronounced for the 20 segments of the grafted branch for the B20 chains (not in Figure 6), and even more for the 10 segments of the grafted branch of the B10 chains.

The orientation of segments, together with the density of the end groups, and the distribution of the separation between branches suggest that for high surface coverages the branched chains with a short branch grafted to the surface orgnize themselves in such a way that the short grafted branch stretches as much as possible in order to allow the maximal conformational freedom to the two free branches (see the inset of Figure 2 that shows the distribution of the branching segment at the highest surface coverage for B10 and B20 chains). Moreover, these two free branches seem to be organized such that one is stretched toward the solvent while the other folds toward the grafting wall. In this way, both free branches get a maximal conformational entropy at the cost of the short grafted branched. This seems a reasonable compromise since the grafted branch is shorter than the two free branches, in particular for the B10 chains where the effect is more pronounced.

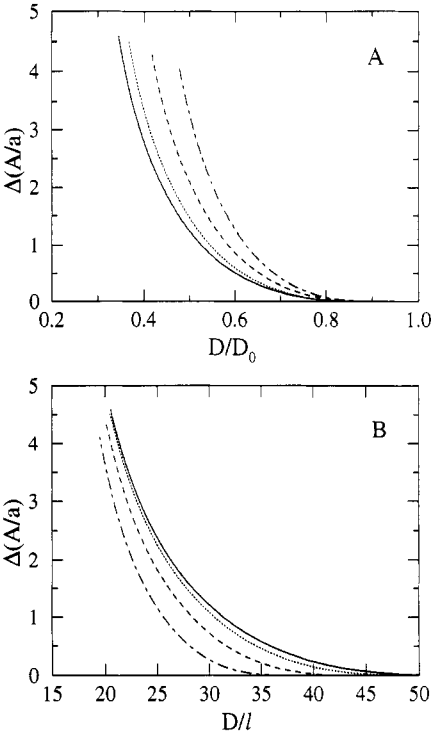

Figure 7. Change in free energy per unit area as function of the distance between two parallel grafted walls for linear, B30, B20, and B10 chains. Lines are as in Figure 2. In (A) the distances are scaled by the onset of the interaction distance, D_0, which corresponds to the minimal distance where the two grafted layers start to feel each other. In (B) the distance is not scaled. The free energy per unit area is measured in $k_B T/l^2$ units.

One of the most important applications of grafted chains is in their ability to stabilize colloidal suspensions. This is due to the repulsive interactions between grafted surfaces in a good solvent environment. We are interested in looking at the changes in the force profiles caused by changes in the chain architecture. The force, as measured with the force-balance apparatus,[39] can be shown to be, within the Derjaguin approximation,[40] the change in free energy per unit area upon changing the distance between the two grafted plates. This can be obtained directly using eq 11 as a function of the distance between two surfaces grafted with chain molecules. However, in order to do so one needs to take into consideration the fact that now the volume fraction term in the constraint equations has to include contributions from polymers arising from the two parallel surfaces. Namely, eq 2 now reads

$$\langle \phi_p(z) \rangle = \sigma(\langle n_1(z) \rangle + \langle n_2(z) \rangle) v_0 \qquad z \geq 0 \qquad (15)$$

where $\langle n_{1(2)}(z) \rangle$ represents the average number of segments that the polymers arising from surface 1 (2) have in layer z. Note that the form of the pdf of chain conformations for the two surfaces has exactly the same functional form as described by eq 7, but now the osmotic pressure depend on the solution of the modified constraint equations.

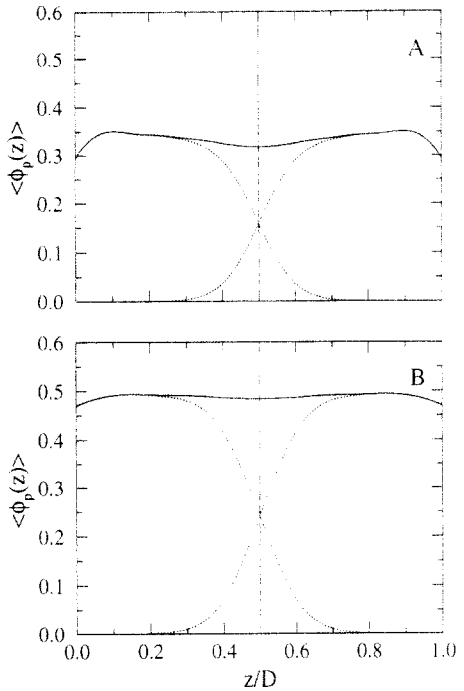

Figure 8. Total polymer density (full lines) and the polymer density from each grafted surface (dotted lines) as a function of the scaled distance between two interacting grafted walls for (A) linear chains and (B) B10 chains, both for $\sigma = 0.10$ and $D = D_0/2$. The distance is scaled by the total separation between the two grafting walls. The dashed line marks the midplane between the two brushes. Note the amount of interdigitation in the two cases (see text).

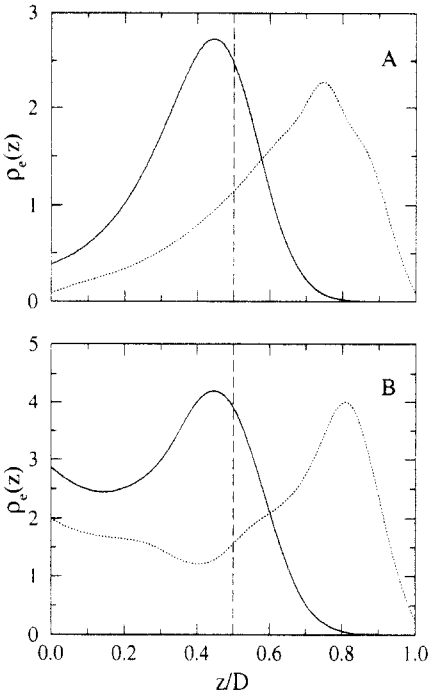

Figure 9. End segment distribution as a function of the scaled distance for the same conditions as in Figure 8 (full lines) and for the case of the single grafted wall (dotted lines). Note the marked shifted of the profiles in the interacting brushes, even though they correspond to the same grafting density.

Figure 7A shows the force profiles as a function of the distance between the two grafted plates for the linear, B30, B20, and B10 chains all for $\sigma = 0.10$. The distance is normalized by the distance between the two plates at the onset of interactions. They are $D_0/l = 60$, 56, 48, and 41 for linear, B30, B20, and B10, respectively. The most important result from the figure is that the slopes of the profiles are sharper the shorter the grafted branch. Note also (Figure 7B) that for the short grafted branch chains the interactions are of shorter range, reflecting the fact that the most extended chains are shorter. These results may show interesting applications in colloidal stabilization by branched chains, because the range and the slope of the interaction potentials can be modified by the chain architecture.

The reason for the sharper force profiles, at fixed surface coverage, for the branched chains can be understood by looking at the segment density profiles for the two interacting layers when they are at distance $D = D_0/2$. This is shown in Figure 8 for the linear and B10 chains. The full lines are the total density profile, and the dotted lines represent the density profiles of the chains from each grafting surface. In the linear and B10 chains the profiles show the same qualitative behavior, namely, an initial slight increase of segment density close to the grafting surfaces and then a slight dip in the midplane. However, the absolute value of the density is much higher in the B10 chains, resulting in larger repulsions. This again reflects the bulkier character of the branched chains as compared to the linear ones. The profiles also indicate the amount of interdigitation of the chains into the opposite monolayer. In both cases a significant amount of interdigitation is observed. For this particular case 7.6% of the B10 chains are interdigitating as compared to 6.4% in the case of the linear chains.

The interactions between the interpenetrating layers also change the molecular organization of the chains. This can be seen in the density of end segments as a function of the distance from the grafting surface. Figure 9 shows these profiles for linear and B10 chains, again for $\sigma = 0.10$. The full lines correspond to the case of two layers at $D = D_0/2$, and the dotted lines are for the same surface coverage but without the opposite layer, i.e. $D > D_0$. In both cases the end segments are strongly shifted toward the grafting surface due to the repulsions of the opposite brush. Thus, there is a large increase in the number of end groups near the grafting wall. This effect is more pronounced for the branched chains. There is relatively the same probability of the end groups to penetrate into the other layer for linear and B10 chains in this case. Note also that the B10 molecules interacting with another brush have the maximum of the distribution at the same distance from the grafting wall where the single branched brush has a local minimum.

We have shown that in the case of a single grafted wall the B10 chains tend to organize such that the probability of the conformations having one free branch toward the solvent and the other folded toward the grafting wall is highly enhanced at large surface coverages. This effect persists in the case of the interacting brushes where we have found that almost all the chains with one free end near the grafting wall have the other free end penetrating into the opposite brush.

Figure 10 shows the orientation profiles for the linear and branched chains for the same cases as above. It is clearly seen in the figure that the conformations that are dominant in the case of the interacting brushes are those for which the molecules are much less stretched, even though the grafting density does not change. The reduction of stretching in the linear and B10 chains seems to be the same when the brushes are at a distance D_0 from each other.

The picture that emerges from these results is that the probability of chain conformations dramatically changes when two brushes interact with each other. The new distribution is a compromise between the tendency of the

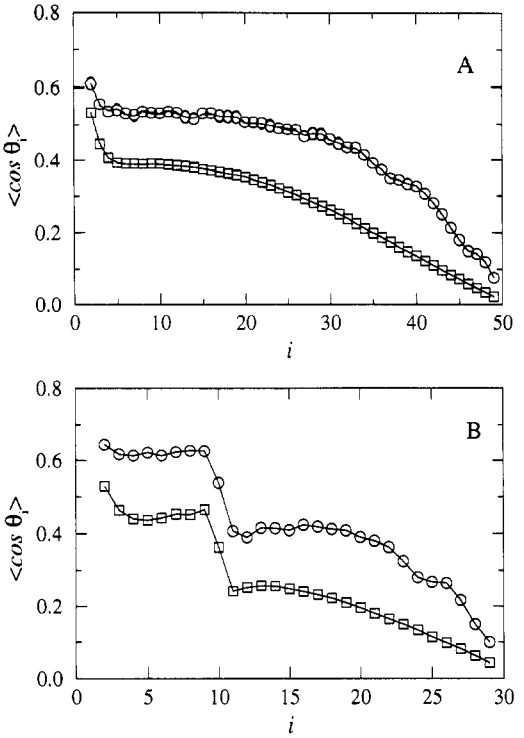

Figure 10. Orientation profiles (see Figure 6) for (A) linear chains and (B) B10 chains all for $\sigma = 0.10$: single brush profile (circles) and brush interacting with a parallel one at distance $D = D_0/2$ (squares).

chains to stretch at the given surface coverage, which is responsible for the interdigitation into the opposite brush, and the repulsion induced by the crowding of the chains arising from the opposite grafted layer. These effects reflect the different ways in which the chains and solvent molecules fill the available volume.

4. Concluding Remarks

We have studied the molecular organization and force profiles of chain molecules of various chain architectures grafted to planar surfaces. The theory is a single-chain mean-field theory in which the chain architecture is introduced through the set of possible single-chain configurations. The theory considers a central chain in the mean field of the interactions with the other polymer chains and solvent molecules. These mean-field interactions are expressed in terms of the osmotic pressures that appear in the probability distribution function of chain conformations and in the solvent density profiles. With one set of single-chain configurations we can find the properties of the film at any desired grafting density by simply solving a set of nonlinear equations. For the case of two interacting layers the constraint equations need to be modified to consider the partition of the available volume to the polymer chains arising from both surfaces and the solvent molecules. Also in these cases the only difference with the single surface calculation is the different set of nonlinear equations to be solved; however the same set of single-chain configurations is needed.

For a given chain architecture the same configurations are used for all grafting densities and distances between walls in the case of parallel layers. Therefore, the different conformational behavior observed as the conditions are varied is fully taken into account by the pdf of chain conformations. This allows us to study in great detail how the probability of conformation varies, and thus, we can obtain a very detailed picture of the effects responsible for the structural changes in the grafted layer.

We have considered linear and three-arm branched chains with one of the arms grafted to the surface. The molecular organization of the branched chains is different from that of the linear chains, in particular for intermediate and high surface coverages. All our calculations were performed for a fixed total number of segments per chain. At very low surface coverages all the chain architectures have as their most probable configurations those that are coil-like. However, as the surface coverage increases the stretching of the chains is different for the different types of molecules. The density profiles for branched chains with a short grafted branch form a brush with higher polymer density near the wall, due to the bulkier structure of the chains. Moreover, the density profile of branched chains at high surface coverage shows a local maximum in density in the position where the branching segment is localized.

The linear chains stretch as the surface coverage is increased, and their end segment distribution has its maximum shifted to larger distances from the wall. Branched chains with short free arms show the same molecular organization as the linear chains. In particular, the shapes of the end segment distributions are almost identical; however, due to the presence of two free ends the density of end segments is doubled for the branched chains as compared to the linear chain. This is in agreement with our previous results on shorter branched chains. The chains with a short branch grafted to the wall show a very different behavior. It is observed that as the surface coverage is increased, the end distribution shows two to three maxima. In the case of the B10 chains one of them is always near the grafting wall and the other near the solvent side of the brush. By looking at different conformational properties, the picture that emerges is that the short grafted branch tends to stretch as much as possible in order to allow the two (longer) free branches as much conformational freedom as possible. In order to achieve that, we have found that the conformations that have one of their free branches toward the grafting wall and the other toward the solvent get a very high probability that increases with surface coverage.

The force profiles between grafted surfaces show the same qualitative behavior for all chain architectures. However, the branched chains have a much steeper profile; namely, they form a more repulsive wall. This wall is at shorter separations due to the intrinsic shorter character of the branched chains. The amount of interdigitation between the layers is large; for a fixed surface coverage and scaled distance it seems to be larger for the branched chains than for the linear ones. Moreover, we have found an increase of the density of end segments near the grafting wall which is more marked for branched chains than for linear ones. For the B10 case, almost all the branched chains that have one of their ends very close to the grafting wall have the other one interpenetrating into the opposite brush.

It will be of interest to experimentally verify our findings. A simple experiment that can be done is the measurement of the force profiles for branched chains and comparison of them to those of the linear ones. If our findings are correct, branched chains may be useful in the design of new colloidal stabilizers with sharp repulsions and a range shorter than that of linear chains, but with the same amount of total polymer segments. Another interesting finding that could be tested experimentally and could be useful in chemical reactions is the significant difference and variety of end distributions found for the branched chains. By functionalizing the free ends, one could look

at chemical reactivity as a function of surface coverage and/or chain architecture. Moreover, by the use of diblock copolymers with one of the blocks branched one can also get interesting heterogeneous catalytical behavior, due to the high density of end groups near the grafting wall, which in the case of diblock copolymers will be a liquid surface.

Acknowledgment. I.S. thanks the Dreyfus Foundation for a Camille and Henry Dreyfus New Faculty Award.

Appendix

In this Appendix we show that the value of the constant in the solvent density profile, eq 8, i.e. the value of the solvent chemical potential, is irrelevant for the pdf of chain conformations as well as for the solvent and polymer density profiles.

Let us first consider the pdf of chain conformations, eq 7. If we add a constant λ to the pressure profiles, namely we consider $\pi'(z) = \pi(z) - \lambda$, we find that the integral in the Boltzmann exponent of the pdf becomes

$$\int_0^\infty dz\, \beta\pi(z)v_0 n_\alpha(z) = \int_0^\infty dz\, \beta\pi'(z)v_0 n_\alpha(z) + \lambda v_0 \int_0^\infty dz\, n_\alpha(z) \quad \text{(A1)}$$

The last term in the righ-hand side of eq A1 is a constant because $\int_0^\infty dz\, n_\alpha(z) = n$, i.e. the length of the chain which is independent of the conformation of the chain. Moreover, that constant term will also appear in the normalization constant, q, and thus $P(\alpha; \{\pi(z)\}) = P(\alpha; \{\pi'(z)\})$.

The next step is to show that the solutions of the constraint equation (1) are independent of the choice of the value of the solvent chemical potential, or any additive constant in the solvent free energy (6). In order to see that it is useful to write the constraint equations to be solved, eq 9, in the following way

$$\sigma \sum_{\{\alpha\}} e^{[-\int_0^\infty dz' \beta\pi(z')v_0 n_\alpha(z')]} (n_\alpha(z)v_0 + e^{-\beta\pi(z)v_0 + \beta\mu_s} - 1) = 0 \qquad z \geq 0 \quad \text{(A2)}$$

which is obtained by multiplying both sides of eq 9 by q as given eq 12. This is in reality the form in which the constraint equations are solved. As can be seen, the solvent density profile as given by $\exp[-\beta\pi(z)v_0 + \beta\mu_s]$ is independent of any choice of μ_s because that will appear as a constant factor multiplying the exponential in the left-hand side of eq A2. This constant term can be taken to the right-hand side of (A2) which, because it is equal to zero, will then have no influence in the solution of the equations.

References and Notes

(1) Rondelez, F.; Ausserre, D.; Hervet, H. *Ann. Rev. Phys. Chem.* **1987**, *38*, 317.
(2) Cosgrove, T.; Heath, T. G.; Phipps, J. S.; Richardson, R. M. *Macromolecules* **1991**, *24*, 94.
(3) Field, J. B.; Toprakcioglu, C.; Ball, R. C.; Stanley, H. B.; Dai, L.; Barford, W.; Penfold, J.; Smith, G.; Hamilton, W. *Macromolecules* **1992**, *25*, 434.
(4) Cosgrove, T.; Heath, T. G.; Ryan, K.; Crowley, T. L. *Macromolecules* **1987**, *20*, 2879.
(5) Auroy, P.; Auvray, L.; Leger, L. *Macromolecules* **1991**, *24*, 2523.
(6) Hadziioannou, G.; Patel, S.; Granick, S.; Tirrell, M. *J. Am. Chem. Soc.* **1986**, *108*, 2869.
(7) Taunton, H. J.; Toprakcioglu, C.; Fetters, L. J.; Klein, J. *Nature (London)* **1988**, *332*, 712.
(8) Kent, M. S.; Lee, L.; Farnoux, B.; Rondelez, F. *Macromolecules* **1992**, *25*, 6240.
(9) Alexander, S. *J. Phys. (Paris)* **1977**, *38*, 977.
(10) Alexander, S. *J. Phys.* (Paris) **1977**, *38*, 983.
(11) de Gennes, P. G. *Macromolecules* **1980**, *13*, 1069.
(12) Dolan, A. K.; Edwards, S. F. *Proc. R. Soc. London, Ser. A* **1974**, *337*, 509.
(13) Dolan, A. K.; Edwards, S. F. *Proc. R. Soc. London, Ser. A* **1975**, *343*, 427.
(14) Scheutjens, J. M. H. M.; Fleer, G. J. *J. Phys. Chem.* **1979**, *83*, 1619.
(15) Scheutjens, J. M. H. M.; Fleer, G. J. *J. Phys. Chem.* **1980**, *84*, 178.
(16) Scheutjens, J. M. H. M.; Fleer, G. J. *Macromolecules* **1985**, *18*, 1882.
(17) Cosgrove, T.; Heath, T.; van Lent, B.; Leermakers, F.; Scheutjens, J. *Macromolecules* **1987**, *20*, 1692.
(18) Milner, S. T.; Witten, T. A.; Cates, M. E. *Europhys. Lett.* **1988**, *5*, 413.
(19) Milner, S. T.; Witten, T. A.; Cates, M. E. *Macromolecules* **1988**, *21*, 2610.
(20) Shim, D. F. K.; Cates, M. E. *J. Phys. (France)* **1989**, *50*, 3535.
(21) Milner, S. T. *Science* **1991**, *251*, 905.
(22) Zhulina, E. B.; Borisov, O. V.; Priamitsyn, V. A. *J. Colloid Interface Sci.* **1990**, *137*, 495.
(23) Zhulina, E. B.; Borisov, O. V.; Brombacher, L. *Macromolecules* **1991**, *24*, 4679.
(24) Murat, M.; Grest, G. S. *Phys. Rev. Lett.* **1989**, *63*, 1074.
(25) Murat, M.; Grest, G. S. *Macromolecules* **1989**, *22*, 4054.
(26) Chakrabarti, A.; Toral, R. *Macromolecules* **1990**, *23*, 2016.
(27) Lai, P.-Y.; Binder, K. *J. Chem. Phys.* **1991**, *95*, 9288.
(28) Dickman, R.; Hong, D. C. *J. Chem. Phys.* **1991**, *95*, 4650.
(29) Halperin, A.; Tirrell, M.; Lodge, T. P. *Adv. Polym. Sci.* **1991**, *100*, 31.
(30) Patel, S. S.; Tirrell, M. *Annu. Rev. Phys. Chem.* **1989**, *40*, 597.
(31) Balachander, N.; Sukenik, C. N. *Langmuir* **1990**, *6*, 1261.
(32) Kurth, D. G.; Bein, T. *Langmuir*, in press.
(33) Napper, Donald H. *Polymeric Stabilization of Colloidal Dispersions*; Academic Press, New York, 1983.
(34) Carignano, M. A.; Szleifer, I. *J. Chem. Phys.* **1993**, *98*, 5006.
(35) Carignano, M. A.; Szleifer, I. *J. Chem. Phys.*, in press.
(36) Flory, P. J. *Statistical Mechanics of Chain Molecules*; Oxford University Press: New York, 1988.
(37) Grest, G. S.; Murat, M. *Macromolecules* **1993**, *26*, 3108.
(38) Wijmans, C. M.; Scheutjens, J. M. H. M.; Zhulina, E. B. *Macromolecules* **1992**, *25*, 2657.
(39) Israelachvili, Jacob. *Intermolecular and Surface Forces*; Accademic Press: London, 1991.
(40) Derjaguin, B. V. *Kolloid Zh.* **1934**, *69*, 155.